ACS APPLIED OPTICAL MATERIALS

Open Access

This article is licensed under CC-BY 4.0

pubs.acs.org/acsaom

Article

A Direct Arylation Approach toward Thermally Activated Delayed Fluorescence-Active Benzo[*c*][1,2,5]thiadiazole Emitters for Near-Infrared Solution-Processed OLEDs

Sonny Brebels,* Emma V. Puttock, Tom Cardeynaels, Kamile Bareikaite, Lucy A. Weatherill, Melissa Van Landeghem, Huguette Penxten, Andrew Danos,* Koen Vandewal, Andrew P. Monkman, Benoît Champagne, and Wouter Maes*

Cite This: *ACS Appl. Opt. Mater.* 2025, 3, 2583−2594

Read Online

ACCESS | Metrics & More | Article Recommendations | Supporting Information

ABSTRACT: An isomeric emitter (**2TPA-iCNBT**) is designed and synthesized, displaying enhanced thermally activated delayed fluorescence (TADF) properties as compared to the reference near-infrared (NIR) emitter TPACNBz (hereafter referred to as **2TPA-CNBT**). Its modified benzo[*c*][1,2,5]thiadiazole-4,7-dicarbonitrile (**iCNBT**) acceptor (A) core positions the two triphenylamine (TPA) donor (D) units adjacently, thereby increasing the D−A torsion angle. Synthesis is realized through the use of an unexploited direct arylation strategy, which, besides offering the desired materials in an efficient and straightforward way, can also yield monofunctionalized emitters (**1TPA-CNBT** and **1TPA-iCNBT**). In total, four emitters are synthesized, characterized, and subsequently compared in terms of their spectroscopic and device properties. Density functional theory is applied to simulate their relative molecular geometry and the arrangement of their (emissive) excited states. Steady-state and time-resolved emission spectroscopy reveal strongly contrasting TADF properties, with **2TPA-iCNBT** exhibiting the largest increase in the photoluminescence quantum yield on removal of oxygen (from 27 to 55%), and the fastest TADF emission kinetics in doped films ($k_{RISC} \sim 10^5$ s^{-1}). In solution-processed organic light-emitting diodes, decent maximum external quantum efficiency (EQE) values are obtained for **2TPA-iCNBT** (2.49%), **1TPA-CNBT** (2.91%), and **1TPA-iCNBT** (2.76%), in clear contrast to **2TPA-CNBT** (1.16%), highlighting the decisive role of the D−A substitution pattern (and the number of D groups) on the performance of NIR-TADF emitters. Furthermore, **2TPA-iCNBT** is shown to maintain the highest EQE at larger current densities (EQE = 1.98% at 10 mA cm^{-2}) within the investigated series, a consequence of its standout TADF behavior.

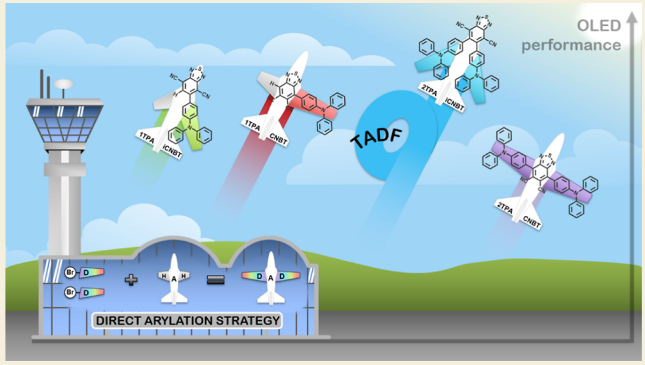

KEYWORDS: *OLEDs, near-infrared, thermally activated delayed fluorescence, direct arylation, solution-processed*

Downloaded via UNIV HASSELT on March 2, 2026 at 10:35:47 (UTC).
See https://pubs.acs.org/sharingguidelines for options on how to legitimately share published articles.

1. INTRODUCTION

The development of organic chromophores with efficient emission in the near-infrared region (NIR; 650−1400 nm)[1] holds significant relevance for emerging applications such as fingerprinting and security, extended (in)visible light communication, spectroscopy, biosensors, and photodynamic therapy.[2−10] The desired NIR wavelength of emission can be achieved by designing chromophores with large π-conjugated systems and/or pronounced charge-transfer (CT) character through the use of strong electron-donating and -accepting moieties.[11] Unfortunately, shifting emission deeper into the NIR is often accompanied by a reduced luminescence due to the "energy gap law", in which the low energy of the excited singlet state increases the nonradiative coupling to the vibrational overtones of the ground state, thus yielding a reduced emission efficiency.[12,13] While this can be counteracted by improving the rigidity of π-conjugated systems (which dampens vibrational modes),[14] such rigidity often leads to the formation of planar structures which are highly susceptible to undesired molecular stacking. In most cases, this gives rise to aggregation-induced quenching, again resulting in a significant loss of the fluorescence efficiency,[15] as well as solubility issues during synthesis and purification.

The limited performance of deep-red and NIR emitters is further exacerbated by poor exciton utilization in conventional

Received: August 6, 2025
Revised: October 5, 2025
Accepted: October 9, 2025
Published: October 20, 2025

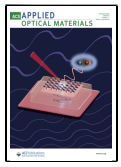

© 2025 The Authors. Published by American Chemical Society

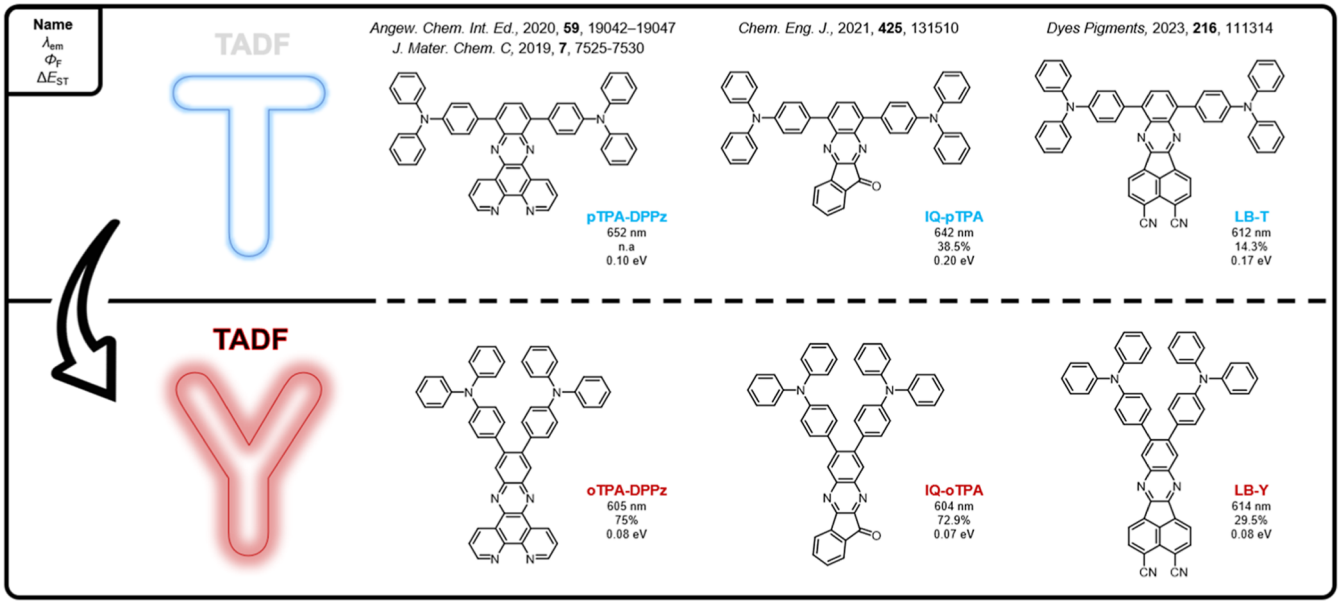

Figure 1. Examples and comparison of reported red T- and Y-shaped TADF emitters. The main emission characteristics (emission wavelength maximum, fluorescence quantum yield, and singlet−triplet energy gap) in doped films are given.

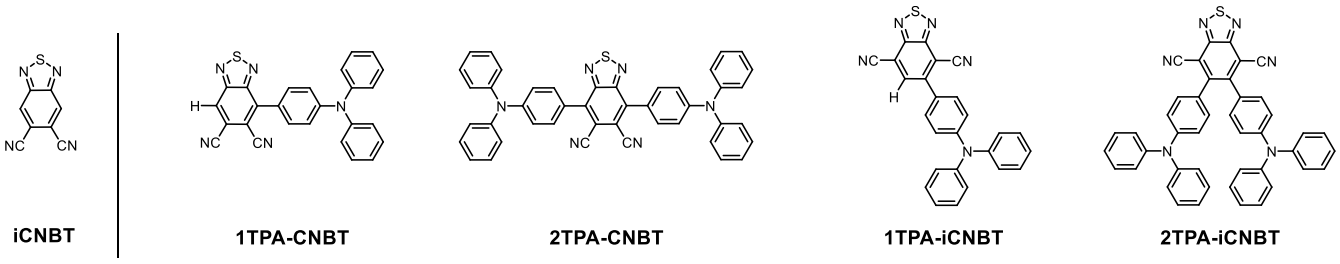

Figure 2. Structural overview of the (i)**CNBT** template and the explored emitters **1TPA-CNBT**, **2TPA-CNBT**, **1TPA-iCNBT**, and **2TPA-iCNBT**.

fluorescence-based electroluminescent devices, which limits their internal quantum efficiency (IQE) to 25%. To overcome this hurdle, much research attention has been focused on the highly promising triplet harvesting mechanism of thermally activated delayed fluorescence (TADF).[16−19] In TADF, excitons from the nonemissive triplet state(s) are upconverted to emissive singlet states via reverse intersystem crossing (RISC), unlocking potential IQEs of up to 100% from injected charges. This spin-flip is promoted by the available thermal energy of the environment, and becomes active when the singlet−triplet energy gap (ΔE_{ST}) is minimized.[20,21] In CT type emitters, TADF behavior can be induced by introducing a twist between electron-donor (D) and electron-acceptor (A) units, which limits the wave function overlap of their respective localized HOMO (highest occupied) and LUMO (lowest unoccupied) frontier molecular orbitals. In this way, a sufficiently small ΔE_{ST} (typically ≤0.2 eV) can be obtained.[22,23] Nonetheless, some degree of orbital overlap is necessary to maintain electronic communication between the D and A units and to permit high emission quantum yields.[24] The small energy gap between states of differing excitonic character ultimately supports efficient RISC, promoting rapid upconversion from the triplet state. This circumvents competitive triplet quenching mechanism in devices, leading to both higher efficiencies and improved stability with reduced efficiency roll-off.[25]

Further structural fine-tuning to maximize the performance of candidate TADF emitters is often explored through the design of different regio-isomers, involving the relocation, addition, or removal of (auxiliary) donor units and/or acceptor groups (e.g. nitriles, fluorines, pyridines).[26−31] For red/NIR-emissive fluorophores containing acceptor moieties with multiple attachment positions available, one strategy entails going from T- to Y-shaped molecules, where the close proximity of the two donor units in the latter is expected to benefit the overall TADF properties.[32−36] This is linked to an increased dihedral angle between the D and A unit(s) due to steric interactions (tuning the HOMO/LUMO overlap), and a better interplay between the relevant singlet and triplet states. For instance, Wang et al. highlighted the beneficial (co)linear orientation of the D and A units in the oTPA-DPPz emitter, resulting in a larger (but still sufficiently small) frontier molecular orbital overlap, which greatly improved the transition probability—as well as the photoluminescence quantum yield (PLQY)—of the emissive CT state.[33] Later, Xie et al. demonstrated how isomeric regulation between ortho- (Y) and para-(T) linkages could effectively switch "on" the TADF mechanism in IQ-oTPA, with the ortho-isomer exhibiting a significantly smaller ΔE_{ST} (and thus efficient TADF), whereas the para-isomer showed only conventional fluorescence.[34] More recently, Liu et al. revealed the presence of an additional, close-lying locally excited (LE) triplet state in the Y-shaped, acenaphtho[1,2-*b*]quinoxaline-3,4-dicarbonitrile-

https://doi.org/10.1021/acsaom.5c00340
ACS Appl. Opt. Mater. 2025, 3, 2583−2594

Scheme 1. Synthesis Protocol for 2TPA-CNBT (3 and 6), 1TPA-CNBT (7), 2TPA-iCNBT (10), and 1TPA-iCNBT (11): (i) (4-(Diphenylamino)phenyl)boronic Acid, $Pd(PPh_3)_4$, K_2CO_3, Toluene, Ethanol, Water, Reflux, 48 h; (ii) KCN, 18-Crown-6, THF, Reflux, 24 h; (iii) CuCN, NMP, 170 °C, 2 h; (iv) 4-Bromo-*N*,*N*-diphenylaniline, $Pd(OAc)_2$, $PtBu_2Me{\cdot}HBF_4$, Pivalic Acid, K_2CO_3, Toluene, Reflux, 24 h; [a] Second Addition of KCN and 18-Crown-6, and Left to Stir for an additional 48 h; [b] 1.1 equiv of 4-Bromo-*N*,*N*-diphenylaniline instead of 2.2

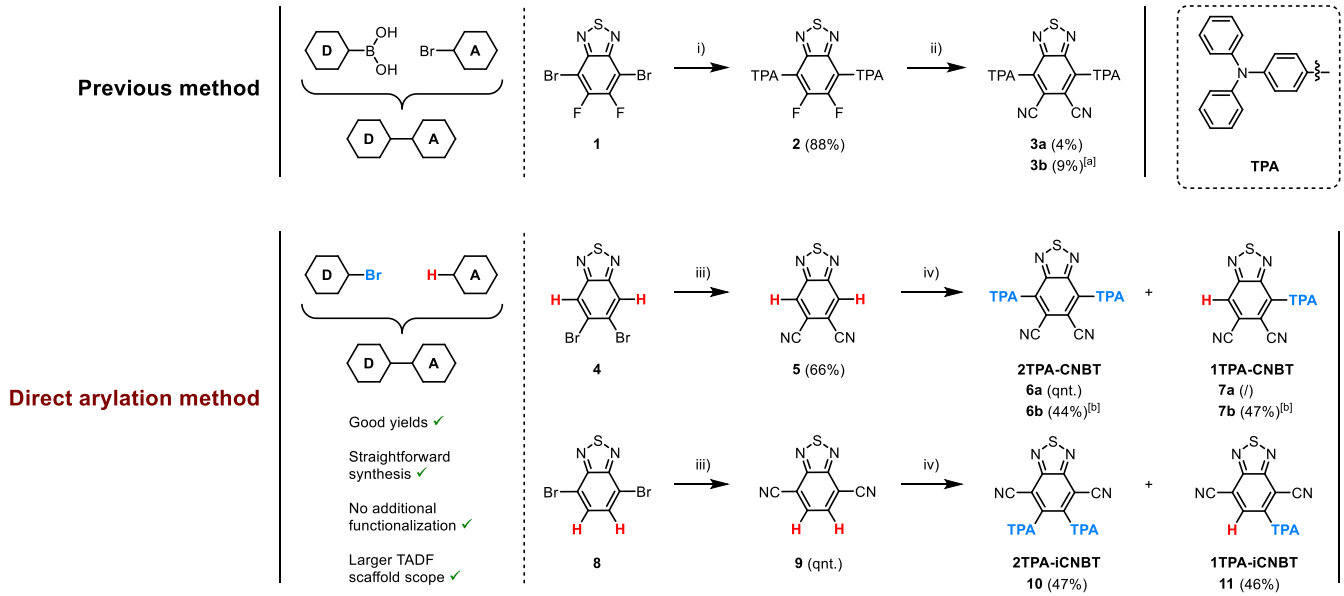

containing LB-Y emitter, and its relevance in improving the TADF process giving rise to faster RISC. The rigid and sterically hindered nature of Y-shaped emitters was also suggested to suppress the nonradiative decay channels that can arise from intramolecular vibrations and rotations, leading to a higher PLQY.[35] A small overview with a few reported examples of T and Y-shaped emitters is given in Figure 1.

In this study, the TADF performance of the previously reported T-shaped emitter 4,7-bis(4-(diphenylamino)phenyl)-benzo[*c*][1,2,5]thiadiazole-5,6-dicarbonitrile (**2TPA-CNBT**)[37] was compared to the novel Y-shaped analog, 5,6-bis(4-(diphenylamino)phenyl)benzo[*c*][1,2,5]thiadiazole-4,7-dicarbonitrile (**2TPA-iCNBT**, Figure 2). These compounds were readily synthesized from commercially available starting products, utilizing a direct arylation strategy as a straightforward method to access the core positions of (i)CNBT. Additionally, this method also allows efficient preparation of the single-donor functionalized fluorophores **1TPA-CNBT** and **1TPA-iCNBT**, enabling comparison of D−A and D−A−D architectures, a topic of similar broad interest (Figure 2).[38−41] To support deeper insight into both individual properties and comparative trends, all compounds were investigated by time-dependent density functional theory (TDDFT) as well as steady-state and time-resolved spectroscopy in solution and doped films, revealing surprising differences in TADF behavior and overall performance. In solution-processed organic light-emitting diode (OLED) devices, the **2TPA-iCNBT** isomer was found to maintain the highest external quantum efficiency (EQE) at higher current densities, correlating to its pronounced delayed fluorescence and short delayed lifetime as measured in 4,4′-bis(*N*-carbazolyl)-1,1′-biphenyl (CBP) films. These results thus showcase our further understanding of isomeric effects and their impact on TADF properties and OLED performance.

2. RESULTS AND DISCUSSION

2.1. Synthesis

A two-step synthetic pathway was previously reported for **2TPA-CNBT**, starting from 4,7-dibromo-5,6-difluorobenzo-[*c*][1,2,5]thiadiazole (Scheme 1).[37] In the first step, the benzo[*c*][1,2,5]thiadiazole core is coupled with a borylated triphenylamine donor unit using a Suzuki−Miyaura cross-coupling reaction. This is followed by a substitution of the fluorine groups with nitriles, using potassium cyanide, yielding the final compound. Unfortunately, several attempts to synthesize **2TPA-CNBT** (**3**) through this method proved largely unsuccessful (Scheme 1). Moreover, such a pathway would not be available for **1TPA-iCNBT** (**10**) and **2TPA-iCNBT** (**11**), since the required (halogenated) precursor is neither commercially available nor easily accessible. Hence, another pathway was developed, employing the direct arylation strategy of Zhang et al.,[42] thereby expanding its scope to include potentially interesting TADF scaffolds. This allowed all four emitters to be obtained in a quick, elegant, and efficient way from cheap and commercially available compounds. Full details on the synthetic procedures and structural characterization data are provided in the Supporting Information.

2.2. Computational Analysis and (TD)DFT Calculations

Density functional theory (DFT) calculations (M06/6-311G[d]) were performed to determine the optimized molecular geometries of **2TPA-CNBT**, **1TPA-CNBT**, **2TPA-iCNBT**, and **1TPA-iCNBT**. Subsequently, two singlet (S_1, S_2) and three triplet (T_1, T_2, T_3) vertical excited state energies (from S_0) were obtained using time-dependent DFT (TDDFT) calculations using a modified LC-BLYP (ω = 0.17 $bohr^{-1}$) exchange−correlation (XC) functional.[43] These calculations were performed under the Tamm−Dancoff approximation[44] (TDA) and the polarizable continuum model (PCM) in methylcyclohexane to simulate a nonpolar environment.[45] The Gaussian16 package was utilized to

https://doi.org/10.1021/acsaom.5c00340
ACS Appl. Opt. Mater. 2025, 3, 2583−2594

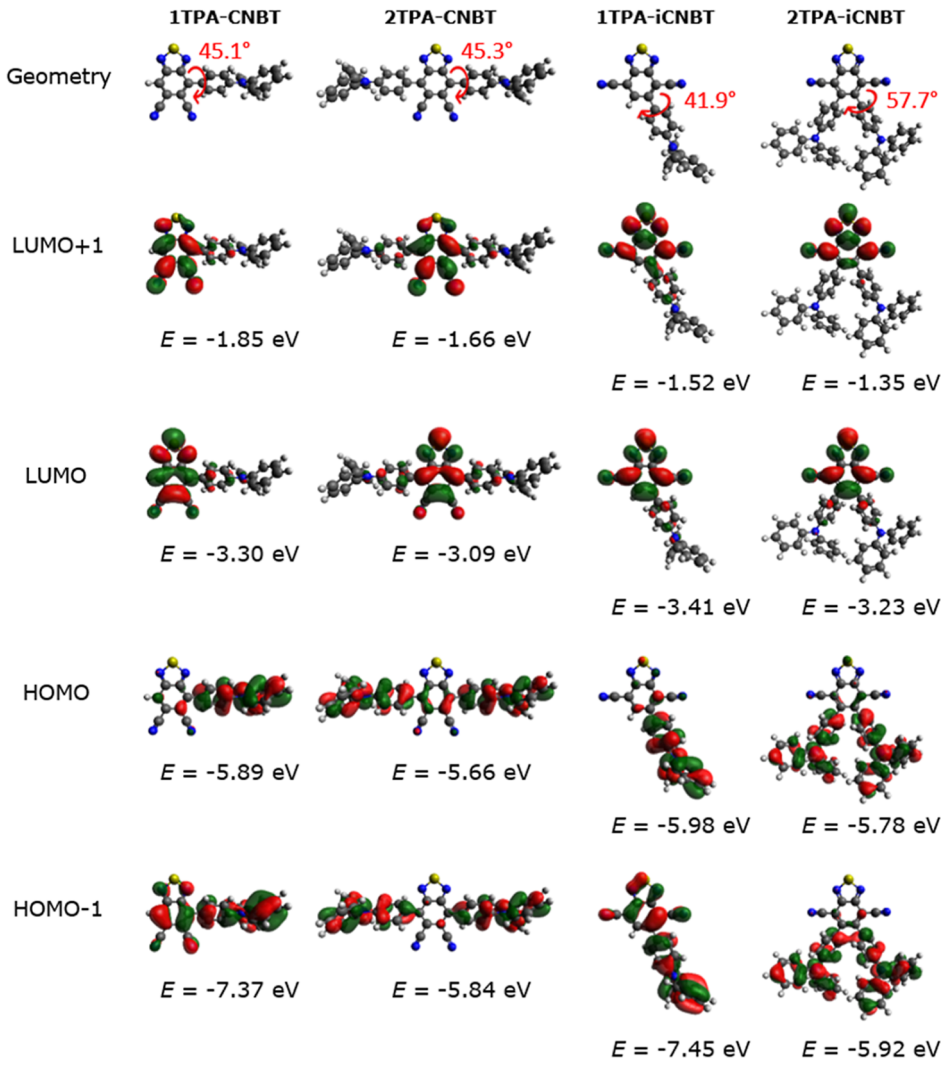

Figure 3. Optimized molecular geometries, energies, and orbital spatial distributions (LUMO + 1, LUMO, HOMO, and HOMO − 1) for **1TPA-CNBT**, **2TPA-CNBT**, **1TPA-iCNBT**, and **2TPA-iCNBT**. Values of dihedral angles are given in red. Isocontour values of 0.02 (au) were used for all orbitals.

perform all calculations.[46] The orbital spatial distributions were obtained from single-point calculations using the same LC-BLYP(17)/6-311G[d] method. The CT character of the involved states was investigated through electron density difference mapping (EDDM), which shows the changing electron density in a molecule upon a transition from the ground state to a specific excited state. These CT characters are described by the amount of electrons transferred during the transition (q_{CT}), the distance over which the electronic charge is transferred (d_{CT}), and the related change in dipole moment ($\Delta\mu$), calculated as described by Le Bahers and co-workers.[47] The distance over which the electronic charge is transferred is also calculated using the Earth Mover's method ($^{EM}d_{CT}$) as reported by Fraiponts et al.,[48] to correct for the highly symmetric nature of **2TPA-CNBT**. To enable this, electron density was approximated by partial atomic charges using an electrostatic potential (CHelpG) charge model.[49] Changing electron densities in both the donor and acceptor unit are indicative of a CT excited state, while confined changes in the same units (similar molecular distribution) point to an LE state instead. For the dominant excited states, a natural transition orbital (NTO) analysis was also carried out, providing the dominant pairs of particle and hole NTO's.[50] Subsequently, to complementary address the LE/CT characters of the transitions, the overlaps between the NTO pairs have been calculated, following the method proposed by Peach and co-workers.[51] The NTO overlap calculations were performed with the Multiwfn program[52] and were represented with ChemCraft.[53] All calculations on the excited states employed the nonequilibrium solvation scheme.[54] Furthermore, the spin−orbit coupling (SOC) matrix elements were evaluated using the PySOC program using the same XC functional, basis set, and PCM treatment as described above.[55]

Optimization of the molecular geometries shows relatively similar orientations (and dihedral angles) between the uncrowded TPA and (i)CNBT subunits in **1TPA-CNBT**, **2TPA-CNBT**, and **1TPA-iCNBT** (θ = 40−45°; Figure 3). A noteworthy exception is **2TPA-iCNBT**, where the close proximity of the two TPA units induces an additional steric interaction, resulting in an increase of the dihedral angle to 58°. Meanwhile, very similar molecular orbital distributions are observed in all four materials for the HOMO (localized on the TPA unit) and LUMO/LUMO + 1 (mainly localized on the acceptor). Superimposing the HOMO and LUMO distribu-

https://doi.org/10.1021/acsaom.5c00340
ACS Appl. Opt. Mater. 2025, 3, 2583−2594

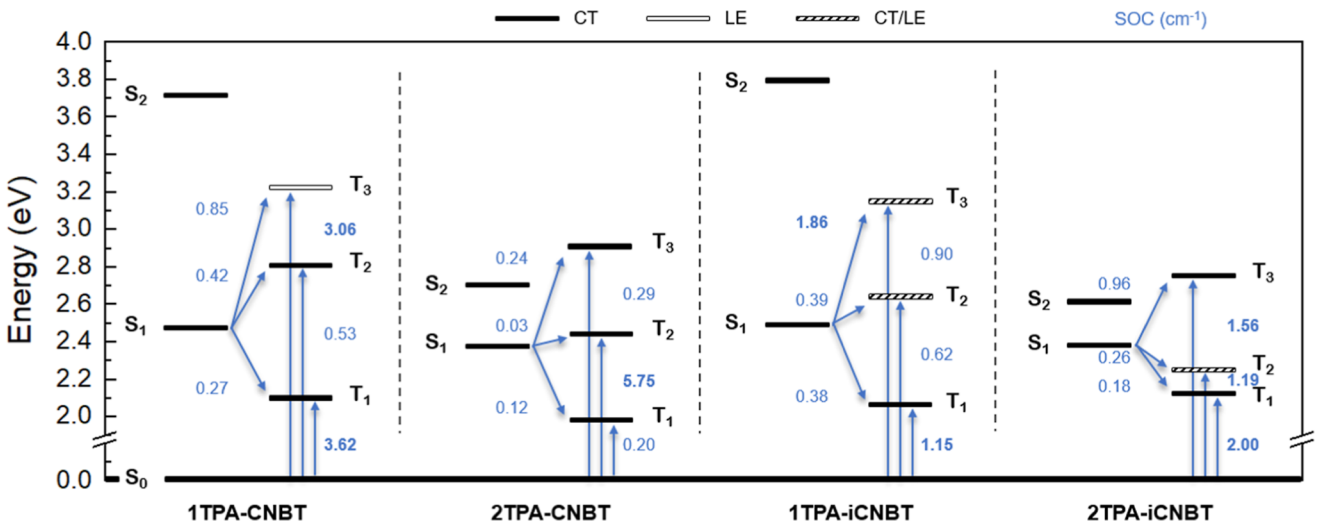

Figure 4. Schematic overview of the excited state energy levels (in eV) of all four emitters with their corresponding CT (black), LE (white), and mixed CT/LE (dashed) character as obtained through TDDFT calculations. Relevant S_0-T_x and S_1-T_x (x = 1−3) couplings and SOC values are shown in blue (SOC values > 1 cm^{-1} in bold).

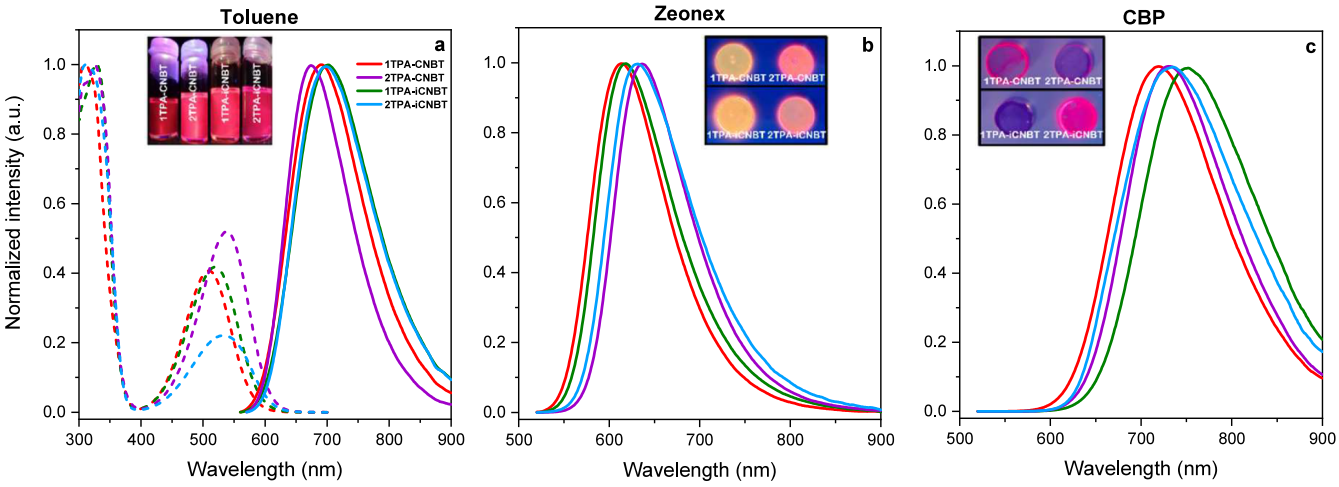

Figure 5. (a) Normalized steady-state absorption (dashed lines) and emission spectra (solid lines) for all four emitters in 10^{-5} M toluene solution (λ_{exc} = 550 nm) and normalized emission spectra for all four emitters in (b) 1 w/w % zeonex and (c) 10 w/w % CBP (λ_{exc} = 500 nm). Pictures show **1TPA-CNBT**, **2TPA-CNBT**, **1TPA-iCNBT**, and **2TPA-iCNBT** in solution and doped films under a 365 nm UV light source.

tions shows a rather limited overlap—which appears to be smallest in **2TPA-iCNBT**—thereby exemplifying the guidelines of typical TADF molecular design. Subsequent TDDFT calculations, EDDMs, and NTO's were employed to assess the properties (i.e. CT nature and relative energy) of the relevant singlet (S_x) and triplet (T_x) excited states (Table S1, Table S2, and Figure S1−S5) Meanwhile, the strength of the spin−orbit coupling could be derived from the calculated SOC matrix elements. A comprehensive excited state energy diagram is shown in Figure 4, and further tabulated in the Supporting Information (Table S2).

For each of the four emitters, the S_1 state is mainly characterized by a HOMO to LUMO transition, indicating a clear CT nature (Table S1). Although this might be less obvious for the S_1 state of **2TPA-CNBT** (which shows a reduced dipole moment as a result of its diametrically oriented TPA units), its CT character becomes apparent when the ${}^{EM}d_{CT}$ and associated EDDM/NTO plots are considered (Figures S1−S5). For S_2, a dominant HOMO − 1 to LUMO transition contributes the most toward the CT nature of each emitter. The main difference here is found in the stabilization of S_2 in **2TPA-CNBT** and **2TPA-iCNBT** compared to **1TPA-CNBT** and **1TPA-iCNBT**, which partly depends on the varying orbital distributions of the HOMO − 1. Importantly, the presence of an identical donor pair in the (symmetric) **2TPA-CNBT** and **2TPA-iCNBT** structures results in nearly degenerate HOMO/HOMO − 1 energy levels, pushing their S_2 state much closer to S_1 when compared to the singlet states of **1TPA-CNBT** and **1TPA-iCNBT**. At the same time, the relative position of the donor unit(s) does not seem to influence the S_1 energy significantly. This is in contrast with the behavior of the higher-lying triplet states, which show a larger dependency on variations in the molecular structure. Increasing the number and/or changing the position of the donor units causes a downward trend in the energy level of T_2 (and T_3), even pushing it below the S_1 state in **2TPA-iCNBT**. For T_1, a clear correlation between its varying energy and any structural changes is less obvious. While rather consistent for **1TPA-CNBT** and **1TPA-iCNBT**, the energy of T_1 appears to vary more significantly among **2TPA-CNBT** and **2TPA-**

https://doi.org/10.1021/acsaom.5c00340
ACS Appl. Opt. Mater. 2025, 3, 2583−2594

Table 1. Spectroscopic and Electrochemical Properties of the Four Emitters

compound	$\lambda_{abs,toluene}$ (nm)[a]	$\lambda_{em,toluene}$ (nm)[b]	$\lambda_{em,zeonex}$ (nm)[c]	$\lambda_{em,CBP}$ (nm)[c]	$\Phi_{F,toluene}$[d] air/inert	$\Phi_{F,zeonex}$[e] air/inert	Φ_{Δ}[f]	HOMO/LUMO (eV)[g]	$\Delta E_{ST,zeonex}$ (eV)[h]
1TPA-CNBT	511	690	613	719	0.27/0.29	0.37/0.48	∼0.45	−5.58/−3.81	[i]
2TPA-CNBT	539	674	636	730	0.78/0.82	0.49/0.50	∼0.15	−5.58/−4.00	0.116
1TPA-iCNBT	516	701	618	752	0.30/0.33	0.57/0.63	∼0.45	−5.57/−3.80	0.143
2TPA-iCNBT	534	698	631	734	0.24/0.28	0.27/0.55	∼0.65	−5.54/−3.99	0.104

[a]CT band absorption maxima in toluene solution. [b]Fluorescence emission maxima in 10^{-5} M toluene solution (λ_{exc} = 550 nm). [c]Fluorescence emission maxima in zeonex (1 w/w %) and CBP (10 w/w %) film (λ_{exc} = 500 nm). [d]Photoluminescence quantum yields in toluene solution under air and inert atmosphere, determined relatively vs Nile blue (Φ_F = 0.27, λ_{exc} = 550 nm in ethanol). [e]Absolute photoluminescence quantum yields in zeonex determined using an integrating sphere under air and inert atmosphere at RT (λ_{exc} = 500 nm). [f]Singlet oxygen quantum yields in toluene solution estimated vs Rose Bengal (Φ_Δ = 0.86, λ_{exc} = 525 nm in ethanol) by monitoring the absorbance of 1,3-diphenylisobenzofuran at 414 nm under emission from a secondary light source. [g]Determined from cyclic voltammetry (Figure S10). [h]The 80 ms delay-time spectra of **2TPA-CNBT**, **1TPA-iCNBT**, and **2TPA-iCNBT** contain multiple emission bands, therefore ΔE_{ST} was estimated from the difference between the peak wavelength maxima of the steady-state fluorescence band at RT and the 80 ms delay-time phosphorescence band at 80 K (Figure S11). [i]Could not be unequivocally determined due to the nature of the 80 ms delay-time spectrum.

iCNBT, seemingly depending on the relative proximity and orientation of their TPA donor units. Naturally, this behavior has a profound effect on the resulting ΔE_{ST} and on TADF performance. Comparing the different emitters, the theoretical ΔE_{ST} decreases from 0.44 eV in **1TPA-iCNBT** and 0.40 eV in **2TPA-CNBT**, down to 0.36 eV in **1TPA-CNBT** and finally 0.26 eV in **2TPA-iCNBT** (Table S2). Consideration should also be given to the role of spin−orbit coupling. According to the El-Sayed rule, spin−orbit coupling more readily enables (R)ISC when it occurs between states which have different natures (e.g. ^{1}CT and ^{3}LE).[56,57] Additionally, the RISC is further enhanced through vibronic coupling (VC) of the T_1 state with other close-lying triplet states.[14,58,59] Although relatively larger estimated SOC values (between S_1 and T_1, T_2 and T_3) are derived for **1TPA-iCNBT** and **1TPA-CNBT**, the absence of LE or hybrid (CT/LE) triplet states below or close to S_1 effectively limits RISC, resulting in weaker TADF. Meanwhile, an even worse delayed fluorescence contribution is expected for **2TPA-CNBT**, owing to the poor SOC between its excited states. However, a small SOC value for the ISC (S_1 to T_1) and the transition to the ground state (T_1 to S_0) does suggest a more suppressed triplet formation in **2TPA-CNBT**. Finally, **2TPA-iCNBT** shows promising potential as the computational investigation reveals a relatively narrow ΔE_{ST}, a hybrid triplet state (T_2) in close proximity of both S_1 and T_1, and improved SOC values compared to **2TPA-CNBT**. This would enable upconversion from T_1 (CT)/T_2 (CT/LE) to S_1 (CT) through a combination of SOC and VC, possibly resulting in a good overall TADF performance.[58,60]

2.3. Photophysical Characterization

Steady-state absorption and emission spectra were measured in solution and doped films to experimentally probe the excited state properties. In toluene solution, very similar high-energy absorption bands are observed around 320 nm, attributed to the π−π^* transition of the TPA moiety (Figure 5a).[37] Meanwhile, CT absorption bands are observed around 515 or 535 nm, for **1TPA-(i)CNBT** and **2TPA-(i)CNBT**, respectively. The red-shift of this band in the disubstituted compounds logically results from the larger conjugated system, which lowers the energy of the excited states. The relative intensity of the CT bands varies significantly, showing the strongest CT absorption for **2TPA-CNBT**. This is in agreement with its calculated oscillator strength, which is nearly double that of the other emitters (Figures S6 and S7, and Table S2).

Meanwhile, the emission spectra in toluene are similar for each emitter, with exception of the slightly blue-shifted emission peak of **2TPA-CNBT** (Figure 5a). This is likely due to its overall weaker dipole moment (change) in the excited state—owing to its more centrosymmetric nature—resulting in weaker solvent stabilization of the emissive S_1 state (Table S2). The CT nature of the emissive singlet state was further investigated through an analysis of the solvatochromic behavior in solvents with different polarities (Figure S9 and Table S3). The increased broadness and significantly red-shifted emission in the more polar solvents confirms the CT character of S_1, as suggested by the TDDFT calculations.

Next, the photoluminescence quantum yields (PLQYs) were determined in toluene under inert ($\Phi_{F\ inert}$) and ambient ($\Phi_{F\ air}$) atmosphere (Table 1). Contrary to the excellent PLQY of **2TPA-CNBT** ($\Phi_{F\ air}$ = 0.78), only moderate values were obtained for **1TPA-CNBT** ($\Phi_{F\ air}$ = 0.27), **1TPA-iCNBT** ($\Phi_{F\ air}$ = 0.30), and **2TPA-iCNBT** ($\Phi_{F\ air}$ = 0.24). The intense fluorescence of **2TPA-CNBT** likely arises due to the limited triplet formation (vide infra), as indicated by the low SOC values between S_1 and T_1 (weak ISC). Surprisingly, no significant changes in the PLQY were observed for any of the emitters under an inert atmosphere, indicating subdued TADF behavior in toluene solution. While seemingly disagreeing with the previous observations of Kumsampao et al. ($\Phi_{F\ inert} \approx 1$ for **2TPA-CNBT** in degassed toluene solution),[37] poor TADF in solution might be expected, since the calculated ΔE_{ST} values are relatively large.

To further investigate the population of triplet states in (toluene) solution, the singlet oxygen quantum yield (Φ_Δ) was measured under ambient conditions. An inverse trend was found for Φ_Δ versus Φ_F, with **2TPA-CNBT** ($\Phi_\Delta \approx 0.15$) exhibiting a relatively low singlet oxygen quantum yield against the higher values of **1TPA-CNBT** ($\Phi_\Delta \approx 0.45$), **1TPA-iCNBT** ($\Phi_\Delta \approx 0.45$), and especially **2TPA-iCNBT** ($\Phi_\Delta \approx 0.65$). Weak ISC and subsequent limited triplet formation in **2TPA-CNBT** follows from the poor SOC between its S_1 and T_1 state, which has noticeably improved in **1TPA-CNBT** and **1TPA-iCNBT**. On the other hand, the ISC of **2TPA-iCNBT** is expected to be the strongest due to the presence of a hybrid triplet state, despite its moderate (<1.0) SOC value. As such, the higher singlet oxygen quantum yield of **2TPA-iCNBT** is indicative of the effective formation of (longer-lived) triplet states in solution.

Next, doped films of zeonex (1 w/w %) and CBP (10 w/w %) were prepared to investigate the photophysical behavior of

https://doi.org/10.1021/acsaom.5c00340
ACS Appl. Opt. Mater. 2025, 3, 2583−2594

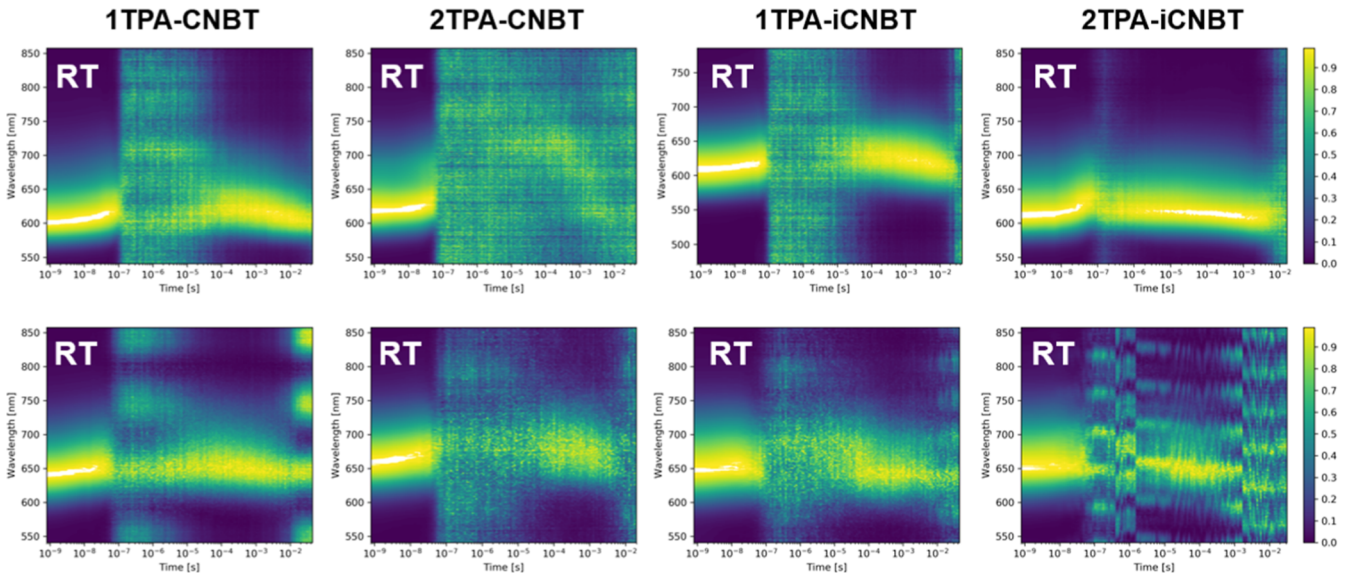

Figure 6. Normalized time-resolved emission spectra (contour plots) for all four isomers in 1 w/w % zeonex films (top row) and 10 w/w % CBP films (bottom row) at RT (λ_{exc} = 355 nm).

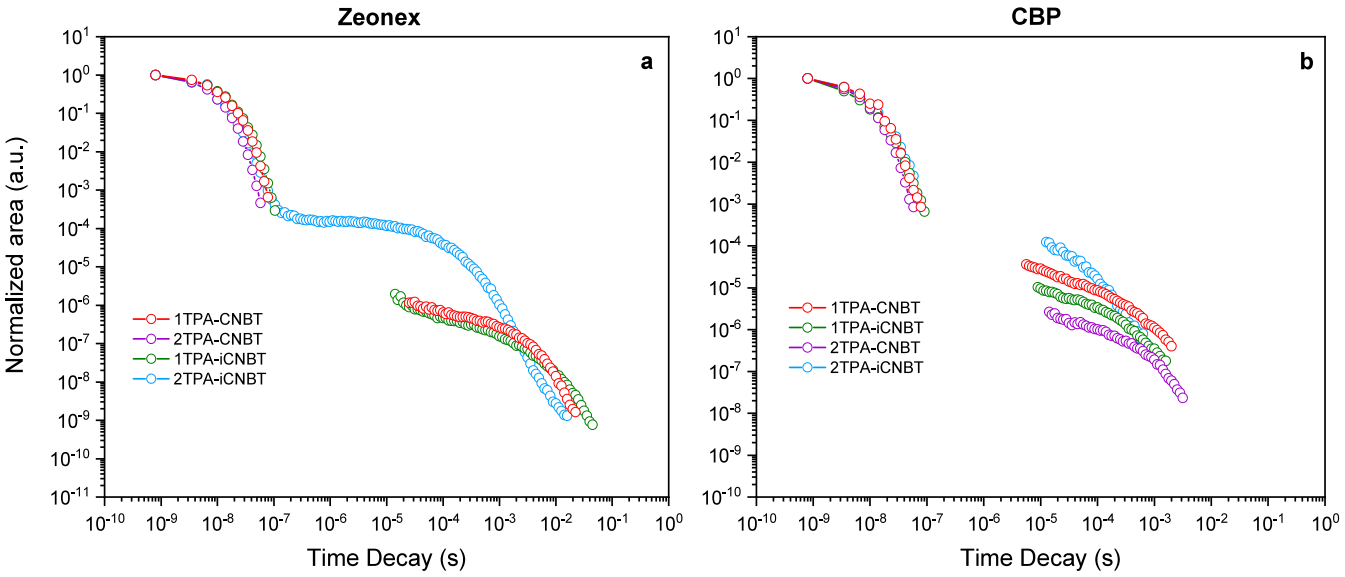

Figure 7. Total emission decay (calculated via the integrated area under the emission curve) for **1TPA-CNBT**, **2TPA-CNBT**, **1TPA-iCNBT**, and **2TPA-iCNBT** at RT in (a) 1 w/w % zeonex and (b) 10 w/w % CBP films. Data points with signal below the noise baseline (normalized to "flat" vertical traces in contour plots) have been omitted from the kinetics decay figures.

the emitters in different solid-state hosts. Zeonex (a nonpolar polymer host) is often used to characterize the intrinsic emission behavior in film, without the influence of strong aggregation or secondary host effects (e.g. CT state stabilization and charge transport). Zeonex also has a low polarizability (comparable to methylcyclohexane),[61] thus introducing only a marginal shift with respect to the gas-phase/isolated molecule emission. **2TPA-CNBT** and **2TPA-iCNBT** show slight bathochromic shifts in their zeonex emission compared to **1TPA-CNBT** and **1TPA-iCNBT** (Figure 5b), relating to their larger conjugated system and reduced singlet energies (Figure 4). At the same time, the PLQY and TADF contribution (based on the difference between $\Phi_{F\ air}$ and $\Phi_{F\ inert}$) steadily improve by moving from toluene to zeonex, with the notable exception of **2TPA-CNBT** (Table 1). **1TPA-iCNBT** shows an overall better performance than **1TPA-CNBT**, giving rise to a higher quantum yield under both ambient ($\Phi_{F\ air}$ = 0.57 vs 0.37) and inert ($\Phi_{F\ inert}$ = 0.63 vs 0.48) conditions. Surprisingly, similar quantum yields are achieved for **2TPA-iCNBT** ($\Phi_{F\ inert}$ = 0.55) and **2TPA-CNBT** ($\Phi_{F\ inert}$ = 0.50) under an inert atmosphere, despite their inherent differences in triplet harvesting. For **2TPA-CNBT**, this can be attributed to the high intrinsic PLQY, which is somewhat maintained in zeonex ($\Phi_{F\ air}$ = 0.49). Meanwhile, the lower efficiency of **2TPA-iCNBT** under air ($\Phi_{F\ air}$ = 0.27) is compensated by the stronger TADF properties, resulting in a doubling of the PLQY on removal of triplet-quenching oxygen. In CBP (a moderately nonpolar small-molecule host), a significant red-shift in the emission of all four emitters is observed (to >700 nm), owing to the stronger stabilization of the emissive CT state (Figure 5c). Interestingly, **1TPA-iCNBT** shows the longest photoluminescence wavelength, strongly

https://doi.org/10.1021/acsaom.5c00340
ACS Appl. Opt. Mater. 2025, 3, 2583−2594

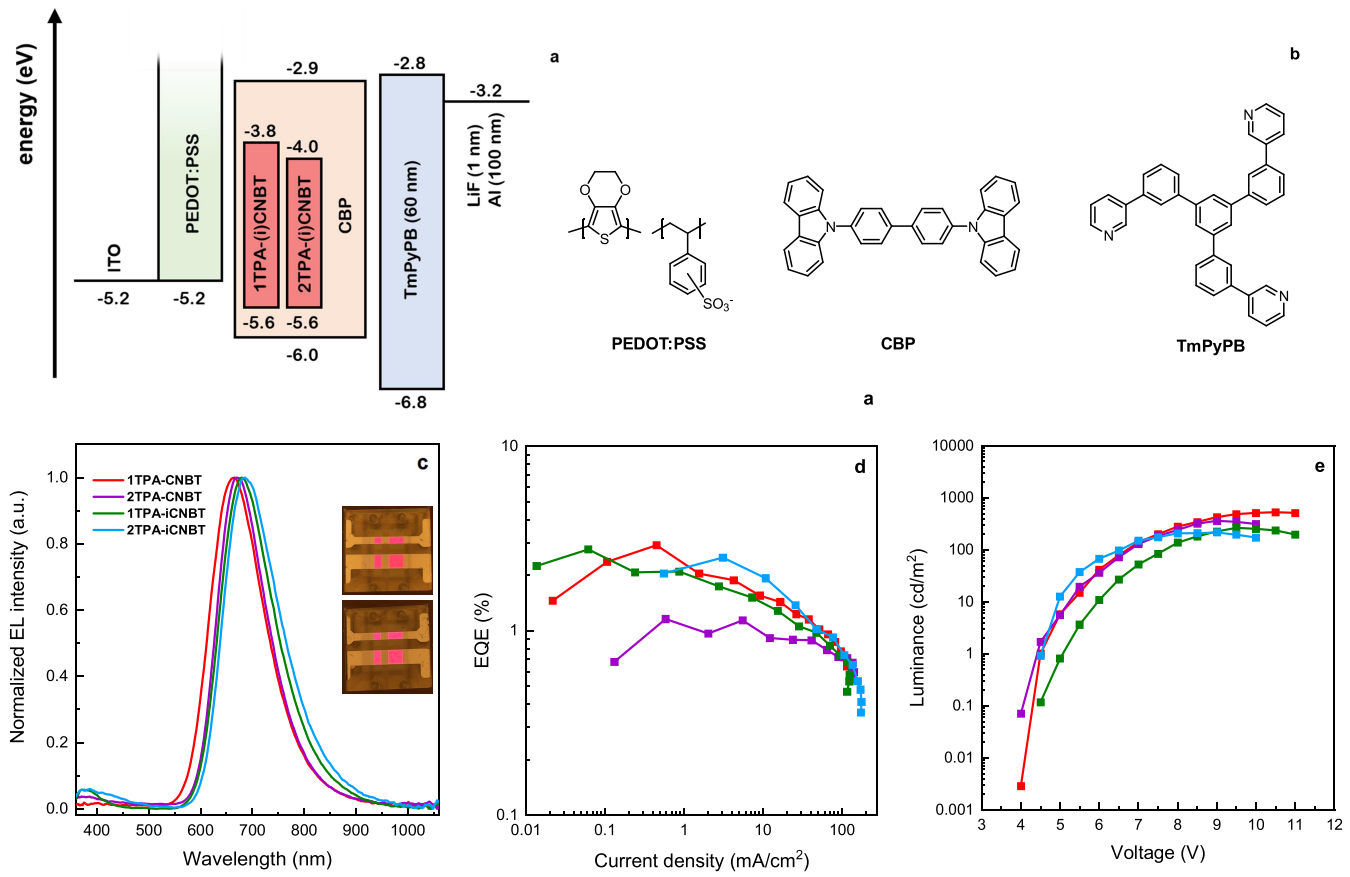

Figure 8. (a) Energy level diagram of the materials employed in the devices. (b) Molecular structures of the materials used in the devices. (c) EL spectra with photographs of the **1TPA-iCNBT** (top) and **2TPA-iCNBT** (bottom) solution-processed OLED devices. (d) EQE-current density curves, and (e) luminance versus voltage plots of the four doped (10 w/w % in CBP) SP-OLED devices.

contrasting the behavior of its isomeric counterpart **1TPA-CNBT**. However, this may also be attributed to a subtle difference in their aggregation behavior in conjunction with their higher concentrations in the CBP host, affecting the solid-state ordering and/or film quality of both emitters.

Time-resolved emission spectroscopy (TRES) experiments were carried out at room temperature (RT) and 80 K to investigate the delayed fluorescence behavior in doped films (Figures 6, 7, and S12−S14). TRES contour plots of the normalized emission spectra illustrate how the emission changes with respect to wavelength across different time scales, allowing the characterization of prompt (10^{-9}−10^{-7} s) and delayed (10^{-7}−10^{-2} s) fluorescence components. At RT, phosphorescence (10^{-3}−10^{3} s) is typically outperformed by nonradiative decay (e.g. molecular vibrations) and therefore too weak to be observed. Hence, measurements were also performed at 80 K to limit vibrational energy losses and suppress TADF emission, enabling us to determine the experimental T_1 energy and ΔE_{ST} (Table 1, Figure S11 and S14).

Prompt fluorescence with a similar intensity and lifetime (up to 100 ns) can be observed for each of the four emitters at RT in zeonex. A small red-shift can be seen toward the end of this time window, which is characteristic of slower decay from lower-energy singlet states of molecules in the film, which likely results from slightly altered dihedral angles between the donor and acceptor units. This shift intensifies at 80 K (Figure S14), as the rotational freedom of the TPA unit is further restricted.[62,63] At RT, delayed fluorescence can be clearly observed (at the same wavelength as the prompt emission) for **1TPA-CNBT**, **1TPA-iCNBT**, and especially **2TPA-iCNBT**. The latter maintains a relatively strong delayed emission for most of the measurement (linked to its small ΔE_{ST} value), while the signal drops below the detection limit of the instrument during the early microsecond time window for **1TPA-CNBT** and **1TPA-iCNBT**. Meanwhile, **2TPA-CNBT** exhibits a delayed fluorescence contribution that barely rises above the instrument baseline at RT in zeonex. This TADF behavior aligns well with the improvement in PLQY under inert conditions, as previously discussed.

TRES measurements were similarly performed for doped CBP films at RT (Figure 6). While the captured delayed fluorescence intensity is weaker, likely due to the reduced thickness of the CBP films, there is a clearer progression in the quantity and kinetics of delayed emission for each material (Figure 7), with **2TPA-iCNBT** being the standout candidate emitter. To derive the kinetic parameters for **2TPA-iCNBT**, its decays were fitted using a kinetic model (Figure S15),[64] which gave rate constants of 3.7 (2.8) × 10^7 s^{-1}, 5.4 (3.9) × 10^6 s^{-1}, and 0.45 (1.1) × 10^5 s^{-1} for the rates of fluorescence, ISC, and RISC in zeonex (and CBP), respectively.

Despite the general similarities in the molecular structure and identical donor fragments, widely different emission behavior was established for each of the four emitters. **2TPA-CNBT** seemingly acts as a typical fluorescent dye, showcasing strong inherent fluorescence in solution and film but a limited capacity for TADF, in contrast with the reported literature.[37] Interestingly, **1TPA-CNBT** demonstrates an

https://doi.org/10.1021/acsaom.5c00340
ACS Appl. Opt. Mater. 2025, 3, 2583−2594

overall better performance in film, exhibiting the second best TADF performance while maintaining a similar solid-state PLQY to **2TPA-CNBT**. Continuing, **2TPA-iCNBT** shows the largest increase in PLQY under an inert atmosphere and maintains the strongest delayed fluorescence intensity and fastest decays, clearly standing out as the best TADF emitter among the investigated compounds. This improved performance is likely supported by the close proximity of a hybrid ^{3}LE/CT state which contributes to the VC (T_2 in Figure 4), thereby promoting the RISC process.[59] As for the CNBT-based emitters, the removal of one donor greatly impacts the capacity for TADF in terms of the ΔE_{ST} and delayed fluorescence intensity, as observed for **1TPA-iCNBT**.

2.4. OLED Device Fabrication and Characterization

Encouraged by the emissive decays and TADF properties recorded in CBP, solution-processed OLED devices of the four emitters were prepared. Following initial characterization and optimization efforts (Figures S16, S17, and Table S5), notable improvement in the device performance was achieved using a stack consisting of ITO/PEDOT:PSS/emitter:CBP (10 w/w %)/TmPyPB (60 nm)/LiF (1 nm)/Al (100 nm) as shown in Figure 8. Water-soluble poly(3,4-ethylenedioxythiophene)/polystyrenesulfonate (PEDOT/PSS) was selected as a common hole-injection layer for solution-processed devices, since it exhibits good resistance to the organic solvent used during the following deposition of the emissive layer.[65] In this case, the doped emissive layer was deposited by spin-coating (2500 rpm, 1 min) from toluene solution and subsequently annealed at 70 °C for 15 min. Finally, an electron-transporting/hole-blocking layer of 1,3,5-tri[(3-pyridyl)-phen-3-yl]benzene (TmPyPB), an electron-injection layer of LiF, and the Al cathode were deposited by thermal evaporation under vacuum. The electroluminescence (EL) spectra, EQE curves, and luminance versus voltage plots are shown in Figure 8 and the data are summarized in Table 2.

Table 2. EL Characteristics of the Doped (10 w/w % in CBP) Solution-Processed OLEDs Based on the Four Compounds

device	$\lambda_{El,max}$ (nm)[a]	EQE_{max} (%)[b]	EQE_{10} (%)[c]	V_{on} (V)[d]	L_{max} (cd·m^{-2})[e]
1TPA-CNBT	664	2.91	1.51	4.5	531 (10.5 V)
2TPA-CNBT	671	1.16	0.96	4.5	361 (9 V)
1TPA-iCNBT	679	2.76	1.41	4.5	265 (9.5 V)
2TPA-iCNBT	684	2.49	1.98	4.5	216 (9 V)

[a]Maximum electroluminescence peak. [b]Maximum external quantum efficiency at 4.5−5 V. [c]External quantum efficiency at a current density of 10 mA·cm^{-2}. [d]Turn-on voltage. [e]Maximum luminance obtained at a specified voltage (given in parentheses).

Each of the devices displayed deep red and some NIR emission, with an EL peak centered between 664 and 684 nm. Interestingly, the EL spectra are notably blue-shifted compared to the PL spectra in CBP (Figure 5), which may arise from the difference in drying time and thickness between the spin-coated (rapidly dried) and drop-casted (slowly dried) films, respectively. Furthermore, a minor EL signal is found around 400 nm for all devices, which is attributed to the self-emission of the CBP host[66] and/or TmPyPB.[67] The generally low luminance values of the devices arise from the considerable portion of emission falling outside the human visible range (>700 nm) which is therefore not contributing to this metric, although the concurrent emission of significant visible light means that alternative reporting in radiosity units is of similarly limited usefulness.

Devices based on **1TPA-CNBT** exhibited the highest EQE_{max} (2.91%), closely followed by **1TPA-iCNBT** (2.76%), and **2TPA-iCNBT** (2.49%). In contrast, despite its intrinsically high PLQY (which is likely responsible for its comparably high luminance), **2TPA-CNBT** showed the worst EQE_{max} in these solution-processed OLEDs (1.16%). While this seemingly contradicts its reported OLED performance in evaporated devices, it is important to consider the generally inferior performance of solution-processed devices, and that maximum reported EQEs often correspond to the lowest-luminance measurements near the turn-on voltage (i.e. those measurements with the lowest signal-to-noise ratios).[68] Nonetheless, the best overall EQE at moderate current densities (∼10 mA) within this series was maintained by **2TPA-iCNBT**, consistent with its higher delayed emission intensity and faster TADF kinetics in the optical measurements of CBP films. For the other emitters which exhibit slower RISC, the accumulation of triplet excitons more rapidly enables multiexciton quenching processes, leading to a more severe loss of efficiency as the device is driven with higher currents. While there is plenty of room (and need) for further improvements—especially in terms of the NIR emission wavelength range, EQE, and stability—these results contribute to the growing interest in solution-processed NIR-TADF OLEDs, where reported examples remain relatively scarce (Table S6).[10,69,70]

3. CONCLUSIONS

The influence of the relative position and number of triphenylamine donor units on the (delayed) emission properties of **TPA-(i)CNBT** was investigated, revealing considerable changes in the emission wavelength, photoluminescence quantum yield, delayed fluorescence rate, TADF efficiency, and solution-processed OLED performance. **2TPA-CNBT**, chosen as the reference compound, showed modest TADF performance. In comparison, the Y-shaped emitter **2TPA-iCNBT** exhibited superior TADF behavior in the solid state, likely owing to its larger dihedral angle between the closely spaced donor units, and the introduction of the **iCNBT** acceptor core which generates close-lying hybrid CT/LE triplet states. At the same time, the TADF behavior changed drastically when one of the donor units was removed. **1TPA-iCNBT** showed a largely reduced TADF performance (and a higher, less oxygen-sensitive PLQY) compared to **2TPA-iCNBT**, which is attributed to a reduced dihedral angle, a larger ΔE_{ST}, and the absence of any apparent LE or hybrid triplet states. Meanwhile, a rather unexpected but significant TADF contribution was found for **1TPA-CNBT**, in clear opposition to **2TPA-CNBT**. Despite exhibiting a similar calculated dihedral angle and simulated ΔE_{ST} to **2TPA-CNBT**, the removal of one donor unit greatly improves the SOC between the S_1 and T_1 excited states of **1TPA-CNBT**, yielding a comparable performance to **1TPA-iCNBT**. All four emitters were prepared in high yields using a direct arylation strategy, enabling the development of previously unattainable TADF scaffolds. In the end, deep-red to near-infrared solution-processed doped OLEDs of **1TPA-CNBT**, **1TPA-iCNBT**, and **2TPA-iCNBT** gave rise to modest EQE_{max} values of 2.91, 2.76, and 2.49%, respectively, with the latter maintaining the highest efficiency at higher driving currents (>10 mA cm^{-2}) and lowest

https://doi.org/10.1021/acsaom.5c00340
ACS Appl. Opt. Mater. 2025, 3, 2583−2594

roll-off within the series. These results demonstrate the importance of investigating varying structural motifs, substitution positions, and especially the role of auxiliary donor units in the development of new TADF emitters, ensuring proper exploration of the underlying design rules and the discovery of more performant isomeric variants.

■ ASSOCIATED CONTENT

Supporting Information

The Supporting Information is available free of charge at https://pubs.acs.org/doi/10.1021/acsaom.5c00340.

Synthetic procedures, (TD)DFT calculations, simulated spectra, analyses of the electronic excitations, additional (time-resolved) absorption and emission spectra, cyclic voltammetry data, device optimization overview, and structural characterization (NMR and MALDI-ToF mass spectrometry) (PDF)

■ AUTHOR INFORMATION

Corresponding Authors

Sonny Brebels − *Institute for Materials Research (IMO-IMOMEC), Hasselt University, Hasselt B-3500, Belgium; IMOMEC Division, IMEC, Diepenbeek B-3590, Belgium;* Email: sonny.brebels@uhasselt.be

Andrew Danos − *Department of Physics, OEM Group, Durham University, Durham DH1 3LE, U.K.; School of Physical and Chemical Sciences, Queen Mary University of London, London E1 4NS, U.K.;* orcid.org/0000-0002-1752-8675; Email: a.danos@qmul.ac.uk

Wouter Maes − *Institute for Materials Research (IMO-IMOMEC), Hasselt University, Hasselt B-3500, Belgium; IMOMEC Division, IMEC, Diepenbeek B-3590, Belgium;* orcid.org/0000-0001-7883-3393; Email: wouter.maes@uhasselt.be

Authors

Emma V. Puttock − *Department of Physics, OEM Group, Durham University, Durham DH1 3LE, U.K.;* orcid.org/0000-0003-3050-7489

Tom Cardeynaels − *Institute for Materials Research (IMO-IMOMEC), Hasselt University, Hasselt B-3500, Belgium; IMOMEC Division, IMEC, Diepenbeek B-3590, Belgium; Laboratory of Theoretical Chemistry, Theoretical and Structural Physical Chemistry Unit, Namur Institute of Structured Matter, University of Namur, Namur B-5000, Belgium*

Kamile Bareikaite − *Department of Physics, OEM Group, Durham University, Durham DH1 3LE, U.K.*

Lucy A. Weatherill − *Department of Physics, OEM Group, Durham University, Durham DH1 3LE, U.K.;* orcid.org/0009-0007-0665-7432

Melissa Van Landeghem − *Institute for Materials Research (IMO-IMOMEC), Hasselt University, Hasselt B-3500, Belgium; IMOMEC Division, IMEC, Diepenbeek B-3590, Belgium;* orcid.org/0000-0001-8927-5358

Huguette Penxten − *Institute for Materials Research (IMO-IMOMEC), Hasselt University, Hasselt B-3500, Belgium; IMOMEC Division, IMEC, Diepenbeek B-3590, Belgium*

Koen Vandewal − *Institute for Materials Research (IMO-IMOMEC), Hasselt University, Hasselt B-3500, Belgium; IMOMEC Division, IMEC, Diepenbeek B-3590, Belgium;* orcid.org/0000-0001-5471-383X

Andrew P. Monkman − *Department of Physics, OEM Group, Durham University, Durham DH1 3LE, U.K.;* orcid.org/0000-0002-0784-8640

Benoît Champagne − *Laboratory of Theoretical Chemistry, Theoretical and Structural Physical Chemistry Unit, Namur Institute of Structured Matter, University of Namur, Namur B-5000, Belgium;* orcid.org/0000-0003-3678-8875

Complete contact information is available at: https://pubs.acs.org/10.1021/acsaom.5c00340

Notes

The authors declare no competing financial interest.

■ ACKNOWLEDGMENTS

The authors thank the Research Foundation—Flanders (FWO Vlaanderen) for financial support (projects G087718N, G0D1521N, I006320N, GOH3816NAUHL, the Scientific Research Community "Supramolecular Chemistry and Materials" (W000620N), postdoctoral fellowship 1284623N (T.C.), postdoctoral fellowship 1270123N (M.V.L.), and PhD scholarship 1SC8621N (S.B.)). The calculations were performed on the computers of the "Consortium des équipements de Calcul Intensif (CÉCI)" (https://www.ceci-hpc.be), including those of the "UNamur Technological Platform of High-Performance Computing (PTCI)" (https://www.ptci.unamur.be), for which we gratefully acknowledge financial support from the FNRS-FRFC, the Walloon Region, and the University of Namur (Conventions No. GEQ U.G006.15, U.G018.19, U.G011.22, RW/GEQ2016, RW1610468, and RW2110213). The project has also received funding from the European Union's Horizon 2021 research and innovation programme under the Marie Skłodowska Curie grant agreement No. 101073045 (TADFsolutions). The authors thank Dr. P. Beaujean for performing the NTO calculations.

■ REFERENCES

(1) Vasilopoulou, M.; Fakharuddin, A.; García de Arquer, F. P.; Georgiadou, D. G.; Kim, H.; Mohd Yusoff, A. R. b.; Gao, F.; Nazeeruddin, M. K.; Bolink, H. J.; Sargent, E. H. Advances in solution-processed near-infrared light-emitting diodes. *Nat. Photonics* **2021**, *15* (9), 656−669.

(2) Minotto, A.; Haigh, P. A.; Łukasiewicz, Ł. G.; Lunedei, E.; Gryko, D. T.; Darwazeh, I.; Cacialli, F. Visible light communication with efficient far-red/near-infrared polymer light-emitting diodes. *Light Sci. Appl.* **2020**, *9*, 70.

(3) Khan, Y.; Han, D.; Pierre, A.; Ting, J.; Wang, X.; Lochner, C. M.; Bovo, G.; Yaacobi-Gross, N.; Newsome, C.; Wilson, R.; Arias, A. C. A flexible organic reflectance oximeter array. *Proc. Natl. Acad. Sci. U.S.A.* **2018**, *115* (47), E11015−e11024.

(4) Lin, C.-H.; Karim, K. S.; Tai, Y.-H. P-130: A Full Screen Biometric Identification Approach for OLED Displays by Using Near-Infrared OLED. *SID Symp. Dig. Tech. Pap.* **2020**, *51* (1), 1855−1858.

(5) Lian, C.; Piksa, M.; Yoshida, K.; Persheyev, S.; Pawlik, K. J.; Matczyszyn, K.; Samuel, I. D. W. Flexible organic light-emitting diodes for antimicrobial photodynamic therapy. *npj Flexible Electron.* **2019**, *3* (1), 18.

(6) Zhang, F.; Tang, B. Z. Near-infrared luminescent probes for bioimaging and biosensing. *Chem. Sci.* **2021**, *12* (10), 3377−3378.

(7) Qi, S.; Kim, S.; Nguyen, V.-N.; Kim, Y.; Niu, G.; Kim, G.; Kim, S.-J.; Park, S.; Yoon, J. Highly Efficient Aggregation-Induced Red-Emissive Organic Thermally Activated Delayed Fluorescence Materials with Prolonged Fluorescence Lifetime for Time-Resolved Luminescence Bioimaging. *ACS Appl. Mater. Interfaces* **2020**, *12* (46), 51293−51301.

(8) Ni, F.; Li, N.; Zhan, L.; Yang, C. Organic Thermally Activated Delayed Fluorescence Materials for Time-Resolved Luminescence Imaging and Sensing. *Adv. Opt. Mater.* **2020**, *8* (14), 1902187.
(9) Xu, M.; Li, X.; Liu, S.; Zhang, L.; Xie, W. Near-infrared organic light-emitting materials, devices and applications. *Mater. Chem. Front.* **2023**, *7* (20), 4744−4767.
(10) Ahadzadeh, S.; Brebels, S.; Maes, W.; Deferme, W. Strategies for Advancing Near-Infrared Organic Light-Emitting Diodes: Innovations in Luminescent Materials, Device Architectures, Fabrication Methods, and Applications. *Adv. Funct. Mater.* **2025**, 2419599.
(11) Yamaguchi, Y.; Matsubara, Y.; Ochi, T.; Wakamiya, T.; Yoshida, Z.-i. How the π Conjugation Length Affects the Fluorescence Emission Efficiency. *J. Am. Chem. Soc.* **2008**, *130* (48), 16442.
(12) Englman, R.; Jortner, J. The energy gap law for radiationless transitions in large molecules. *Mol. Phys.* **1970**, *18* (2), 145−164.
(13) Ghosh, P.; Alvertis, A. M.; Chowdhury, R.; Murto, P.; Gillett, A. J.; Dong, S.; Sneyd, A. J.; Cho, H.-H.; Evans, E. W.; Monserrat, B.; Li, F.; Schnedermann, C.; Bronstein, H.; Friend, R. H.; Rao, A. Decoupling excitons from high-frequency vibrations in organic molecules. *Nature* **2024**, *629* (8011), 355−362.
(14) Paredis, S.; Cardeynaels, T.; Brebels, S.; Deckers, J.; Kuila, S.; Lathouwers, A.; Van Landeghem, M.; Vandewal, K.; Danos, A.; Monkman, A. P.; Champagne, B.; Maes, W. Intramolecular locking and coumarin insertion: a stepwise approach for TADF design. *Phys. Chem. Chem. Phys.* **2023**, *25* (43), 29842−29849.
(15) Hestand, N. J.; Spano, F. C. Expanded Theory of H- and J-Molecular Aggregates: The Effects of Vibronic Coupling and Intermolecular Charge Transfer. *Chem. Rev.* **2018**, *118* (15), 7069−7163.
(16) Yang, Z.; Mao, Z.; Xie, Z.; Zhang, Y.; Liu, S.; Zhao, J.; Xu, J.; Chi, Z.; Aldred, M. Recent advances in organic thermally activated delayed fluorescence materials. *Chem. Soc. Rev.* **2017**, *46*, 915−1016.
(17) Wong, M. Y.; Zysman-Colman, E. Purely Organic Thermally Activated Delayed Fluorescence Materials for Organic Light-Emitting Diodes. *Adv. Mater.* **2017**, *29* (22), 1605444.
(18) Shi, Y.-Z.; Wu, H.; Wang, K.; Yu, J.; Ou, X.-M.; Zhang, X.-H. Recent progress in thermally activated delayed fluorescence emitters for nondoped organic light-emitting diodes. *Chem. Sci.* **2022**, *13* (13), 3625−3651.
(19) Dos Santos, J. M.; Hall, D.; Basumatary, B.; Bryden, M.; Chen, D.; Choudhary, P.; Comerford, T.; Crovini, E.; Danos, A.; De, J.; Diesing, S.; Fatahi, M.; Griffin, M.; Gupta, A. K.; Hafeez, H.; Hämmerling, L.; Hanover, E.; Haug, J.; Heil, T.; Karthik, D.; Kumar, S.; Lee, O.; Li, H.; Lucas, F.; Mackenzie, C. F. R.; Mariko, A.; Matulaitis, T.; Millward, F.; Olivier, Y.; Qi, Q.; Samuel, I. D. W.; Sharma, N.; Si, C.; Spierling, L.; Sudhakar, P.; Sun, D.; Tankelevičiūtė, E.; Duarte Tonet, M.; Wang, J.; Wang, T.; Wu, S.; Xu, Y.; Zhang, L.; Zysman-Colman, E. The Golden Age of Thermally Activated Delayed Fluorescence Materials: Design and Exploitation. *Chem. Rev.* **2024**, *124* (24), 13736−14110.
(20) Adachi, C. Third-generation organic electroluminescence materials. *Jpn. J. Appl. Phys.* **2014**, *53* (6), 060101.
(21) Penfold, T. J.; Dias, F. B.; Monkman, A. P. The theory of thermally activated delayed fluorescence for organic light emitting diodes. *Chem. Commun.* **2018**, *54* (32), 3926−3935.
(22) Im, Y.; Kim, M.; Cho, Y. J.; Seo, J.-A.; Yook, K. S.; Lee, J. Y. Molecular Design Strategy of Organic Thermally Activated Delayed Fluorescence Emitters. *Chem. Mater.* **2017**, *29* (5), 1946−1963.
(23) Chen, X.-K. A Quantum-Chemical Insight into the Role of Charge-Transfer States in Organic Emitters for Electroluminescence. *CCS Chem.* **2020**, *2* (4), 1256−1267.
(24) Tao, Y.; Yuan, K.; Chen, T.; Xu, P.; Li, H.; Chen, R.; Zheng, C.; Zhang, L.; Huang, W. Thermally Activated Delayed Fluorescence Materials Towards the Breakthrough of Organoelectronics. *Adv. Mater.* **2014**, *26* (47), 7931−7958.
(25) Diesing, S.; Zhang, L.; Zysman-Colman, E.; Samuel, I. D. W. A figure of merit for efficiency roll-off in TADF-based organic LEDs. *Nature* **2024**, *627* (8005), 747−753.
(26) Yang, T.; Liang, J.; Cui, Y.; Li, Z.; Peng, X.; Su, S.-J.; Wang, Y.; Li, C. Achieving 34.3% External Quantum Efficiency for Red Thermally Activated Delayed Fluorescence Organic Light-Emitting Diode by Molecular Isomer Engineering. *Adv. Opt. Mater.* **2023**, *11* (1), 2201191.
(27) Shang, A.; Lu, T.; Liu, H.; Du, C.; Liu, F.; Jiang, D.; Min, J.; Zhang, H.; Lu, P. Study of configuration differentia and highly efficient deep-red thermally activated delayed fluorescent organic light-emitting diodes based on phenanthro[4,5-fgh]quinoxaline derivatives. *J. Mater. Chem. C* **2021**, *9* (23), 7392−7399.
(28) Kothavale, S.; Chung, W. J.; Lee, J. Y. Isomer engineering of dipyrido[3,2-a:3′,4′-c]phenazine-acceptor-based red thermally activated delayed fluorescent emitters. *J. Mater. Chem. C* **2022**, *10* (15), 6043−6049.
(29) Kothavale, S.; Lim, J.; Yeob Lee, J. Rational design of CN substituted dibenzo[a,c]phenazine acceptor for color tuning of thermally activated delayed fluorescent emitters. *Chem. Eng. J.* **2022**, *431*, 134216.
(30) Brebels, S.; Cardeynaels, T.; Jackers, L.; Kuila, S.; Penxten, H.; Salthouse, R. J.; Danos, A.; Monkman, A. P.; Champagne, B.; Maes, W. Isomeric modulation of thermally activated delayed fluorescence in dibenzo[a,c]phenazine-based (deep) red emitters. *J. Mater. Chem. C* **2024**, *12* (25), 9255−9265.
(31) Pathak, S. K.; Li, G.; Zhou, C.; Wang, Z.; Liu, H. Regio-isomer enabling efficient red TADF emitters based on pyridobenzoquinoxaline. *J. Mater. Chem. C* **2023**, *11* (20), 6685−6694.
(32) Zhao, B.; Wang, H.; Han, C.; Ma, P.; Li, Z.; Chang, P.; Xu, H. Highly Efficient Deep-Red Non-Doped Diodes Based on a T-Shape Thermally Activated Delayed Fluorescence Emitter. *Angew. Chem., Int. Ed.* **2020**, *59* (43), 19042−19047.
(33) Wang, H.; Zhao, B.; Ma, P.; Li, Z.; Wang, X.; Zhao, C.; Fan, X.; Tao, L.; Duan, C.; Zhang, J.; Han, C.; Chen, G.; Xu, H. A red thermally activated delayed fluorescence emitter employing dipyridophenazine with a gradient multi-inductive effect to improve radiation efficiency. *J. Mater. Chem. C* **2019**, *7* (25), 7525−7530.
(34) Xie, W.; Li, M.; Peng, X.; Qiu, W.; Gan, Y.; Chen, Z.; He, Y.; Li, W.; Liu, K.; Wang, L.; Gu, Q.; Su, S.-J. "On-off" switch between red thermally activated delayed fluorescence and conventional fluorescence by isomeric regulation. *Chem. Eng. J.* **2021**, *425*, 131510.
(35) Liu, B.; Chen, W.-C.; Zhang, R.; Liu, Q.; Wei, H.; Wu, W.-L.; Xing, L.; Wang, R.; Liu, Y.; Ji, S.; Zhang, H.-L.; Huo, Y. Modulating optoelectronic properties of red TADF emitters based on acenaphtho-[1,2-b]quinoxaline-3,4-dicarbonitrile through isomeric engineering. *Dyes Pigm.* **2023**, *216*, 111314.
(36) Zhang, K.; Fan, J.; Wang, C.-K.; Lin, L. Highly efficient T-shaped deep-red thermally activated delayed fluorescence emitters: substitution position effect. *Phys. Chem. Chem. Phys.* **2021**, *23* (38), 21883−21892.
(37) Kumsampao, J.; Chaiwai, C.; Chasing, P.; Chawanpunyawat, T.; Namuangruk, S.; Sudyoadsuk, T.; Promarak, V. A Simple and Strong Electron-Deficient 5,6-Dicyano[2,1,3]benzothiadiazole-Cored Donor-Acceptor-Donor Compound for Efficient Near Infrared Thermally Activated Delayed Fluorescence. *Chem. - Asian J.* **2020**, *15* (19), 3029−3036.
(38) Izumi, S.; Govindharaj, P.; Drewniak, A.; Crocomo, P. Z.; Minakata, S.; de Sousa, L. E.; de Silva, P.; Data, P.; Takeda, Y. Comparative study of thermally activated delayed fluorescent properties of donor−acceptor and donor−acceptor−donor architectures based on phenoxazine and dibenzo[a,j]phenazine. *Beilstein J. Org. Chem.* **2022**, *18*, 459−468.
(39) Barnsley, J. E.; Shillito, G. E.; Larsen, C. B.; van der Salm, H.; Wang, L. E.; Lucas, N. T.; Gordon, K. C. Benzo[c][1,2,5]thiadiazole Donor−Acceptor Dyes: A Synthetic, Spectroscopic, and Computational Study. *J. Phys. Chem. A* **2016**, *120* (11), 1853−1866.
(40) Ye, H.; Yang, J.; Stavrou, K.; Li, M.; Liu, F.; Li, F.; Su, S.-J.; Monkman, A. P. Rational design of dibenzo[a,c]phenazine-derived

https://doi.org/10.1021/acsaom.5c00340
ACS Appl. Opt. Mater. 2025, 3, 2583−2594

isomeric thermally activated delayed fluorescence luminophores for efficient orange-red organic light-emitting diodes. *Dyes Pigm.* **2023**, *219*, 111568.
(41) Haykir, G.; Aydemir, M.; Danos, A.; Gumus, S.; Hizal, G.; Monkman, A. P.; Turksoy, F. Effects of asymmetric acceptor and donor positioning in deep blue pyridyl-sulfonyl based TADF emitters. *Dyes Pigm.* **2021**, *194*, 109579.
(42) Zhang, J.; Parker, T. C.; Chen, W.; Williams, L.; Khrustalev, V. N.; Jucov, E. V.; Barlow, S.; Timofeeva, T. V.; Marder, S. R. C−H-Activated Direct Arylation of Strong Benzothiadiazole and Quinoxaline-Based Electron Acceptors. *J. Org. Chem.* **2016**, *81* (2), 360−370.
(43) Cardeynaels, T.; Paredis, S.; Deckers, J.; Brebels, S.; Vanderzande, D.; Maes, W.; Champagne, B. Finding the optimal exchange−correlation functional to describe the excited state properties of push−pull organic dyes designed for thermally activated delayed fluorescence. *Phys. Chem. Chem. Phys.* **2020**, *22* (28), 16387−16399.
(44) Penfold, T. J. On Predicting the Excited-State Properties of Thermally Activated Delayed Fluorescence Emitters. *J. Phys. Chem. C* **2015**, *119* (24), 13535−13544.
(45) Hirata, S.; Head-Gordon, M. Time-dependent density functional theory within the Tamm−Dancoff approximation. *Chem. Phys. Lett.* **1999**, *314* (3), 291−299.
(46) Frisch, M. J.; Trucks, G. W.; Schlegel, H. B.; Scuseria, G. E.; Robb, M. A.; Cheeseman, J. R.; Scalmani, G.; Barone, V.; Petersson, G. A.; Nakatsuji, H.; Li, X.; Caricato, M.; Marenich, A. V.; Bloino, J.; Janesko, B. G.; Gomperts, R.; Mennucci, B.; Hratchian, H. P.; Ortiz, J. V.; Izmaylov, A. F.; Sonnenberg, J. L.; Williams; Ding, F.; Lipparini, F.; Egidi, F.; Goings, J.; Peng, B.; Petrone, A.; Henderson, T.; Ranasinghe, D.; Zakrzewski, V. G.; Gao, J.; Rega, N.; Zheng, G.; Liang, W.; Hada, M.; Ehara, M.; Toyota, K.; Fukuda, R.; Hasegawa, J.; Ishida, M.; Nakajima, T.; Honda, Y.; Kitao, O.; Nakai, H.; Vreven, T.; Throssell, K.; Montgomery, J. A., Jr.; Peralta, J. E.; Ogliaro, F.; Bearpark, M. J.; Heyd, J. J.; Brothers, E. N.; Kudin, K. N.; Staroverov, V. N.; Keith, T. A.; Kobayashi, R.; Normand, J.; Raghavachari, K.; Rendell, A. P.; Burant, J. C.; Iyengar, S. S.; Tomasi, J.; Cossi, M.; Millam, J. M.; Klene, M.; Adamo, C.; Cammi, R.; Ochterski, J. W.; Martin, R. L.; Morokuma, K.; Farkas, O.; Foresman, J. B.; Fox, D. J. *Gaussian 16*. Rev. A.03: Wallingford, CT, 2016.
(47) Le Bahers, T.; Adamo, C.; Ciofini, I. A Qualitative Index of Spatial Extent in Charge-Transfer Excitations. *J. Chem. Theory Comput.* **2011**, *7* (8), 2498−2506.
(48) Fraiponts, M.; Maes, W.; Champagne, B. Earth Mover's Charge Transfer Distance: A General and Robust Approach for Describing Excited State Locality. *J. Chem. Theory Comput.* **2024**, *20* (7), 2751−2760.
(49) Singh, U. C.; Kollman, P. A. An approach to computing electrostatic charges for molecules. *J. Comput. Chem.* **1984**, *5* (2), 129−145.
(50) Martin, R. L. Natural Transition Orbitals. *J. Chem. Phys.* **2003**, *118* (11), 4775−4777.
(51) Peach, M. J. G.; Benfield, P.; Helgaker, T.; Tozer, D. J. Excitation energies in density functional theory: An evaluation and a diagnostic test. *J. Chem. Phys.* **2008**, *128* (4), 044118.
(52) Lu, T. A comprehensive electron wavefunction analysis toolbox for chemists, Multiwfn. *J. Chem. Phys.* **2024**, *161* (8), 082503.
(53) *Chemcraft—Graphical Software for Visualization of Quantum Chemistry Computations*, version 1.8, build 682. https://www.chemcraftprog.com.
(54) Improta, R.; Barone, V.; Scalmani, G.; Frisch, M. J. A state-specific polarizable continuum model time dependent density functional theory method for excited state calculations in solution. *J. Chem. Phys.* **2006**, *125* (5), 054103.
(55) Gao, X.; Bai, S.; Fazzi, D.; Niehaus, T.; Barbatti, M.; Thiel, W. Evaluation of Spin-Orbit Couplings with Linear-Response Time-Dependent Density Functional Methods. *J. Chem. Theory Comput.* **2017**, *13* (2), 515−524.
(56) Kim, H. S.; Lee, S. H.; Yoo, S.; Adachi, C. Understanding of complex spin up-conversion processes in charge-transfer-type organic molecules. *Nat. Commun.* **2024**, *15* (1), 2267.
(57) El-Sayed, M. A. Spin—Orbit Coupling and the Radiationless Processes in Nitrogen Heterocyclics. *J. Chem. Phys.* **1963**, *38* (12), 2834−2838.
(58) Etherington, M. K.; Gibson, J.; Higginbotham, H. F.; Penfold, T. J.; Monkman, A. P. Revealing the spin−vibronic coupling mechanism of thermally activated delayed fluorescence. *Nat. Commun.* **2016**, *7* (1), 13680.
(59) Gibson, J.; Monkman, A. P.; Penfold, T. J. The Importance of Vibronic Coupling for Efficient Reverse Intersystem Crossing in Thermally Activated Delayed Fluorescence Molecules. *ChemPhysChem* **2016**, *17* (19), 2956−2961.
(60) Samanta, P. K.; Kim, D.; Coropceanu, V.; Brédas, J.-L. Up-Conversion Intersystem Crossing Rates in Organic Emitters for Thermally Activated Delayed Fluorescence: Impact of the Nature of Singlet vs Triplet Excited States. *J. Am. Chem. Soc.* **2017**, *139* (11), 4042−4051.
(61) Stavrou, K.; Franca, L. G.; Monkman, A. P. Photophysics of TADF Guest-Host Systems: Introducing the Idea of Hosting Potential. *ACS Appl. Electron. Mater.* **2020**, *2* (9), 2868−2881.
(62) Dias, F. B.; Santos, J.; Graves, D. R.; Data, P.; Nobuyasu, R. S.; Fox, M. A.; Batsanov, A. S.; Palmeira, T.; Berberan-Santos, M. N.; Bryce, M. R.; Monkman, A. P. The Role of Local Triplet Excited States and D-A Relative Orientation in Thermally Activated Delayed Fluorescence: Photophysics and Devices. *Adv. Sci.* **2016**, *3* (12), 1600080.
(63) Kelly, D.; Franca, L. G.; Stavrou, K.; Danos, A.; Monkman, A. P. Laplace Transform Fitting as a Tool To Uncover Distributions of Reverse Intersystem Crossing Rates in TADF Systems. *J. Phys. Chem. Lett.* **2022**, *13* (30), 6981−6986.
(64) Haase, N.; Danos, A.; Pflumm, C.; Morherr, A.; Stachelek, P.; Mekic, A.; Brütting, W.; Monkman, A. P. Kinetic Modeling of Transient Photoluminescence from Thermally Activated Delayed Fluorescence. *J. Phys. Chem. C* **2018**, *122* (51), 29173−29179.
(65) Lo, C.-C.; Sudheendran Swayamprabha, S.; Hsueh, T.-C.; Chavhan, S. D.; Yadav, R. A. K.; Lee, J.-R.; Kesavan, K. K.; Chen, S.-Z.; Wang, C.-W.; Jou, J.-H. Modification effect of hole injection layer on efficiency performance of wet-processed blue organic light emitting diodes. *Org. Electron.* **2021**, *92*, 106084.
(66) Song, W.; Lee, J. Y.; Cho, Y. J.; Yu, H.; Aziz, H.; Lee, K. M. Electroplex as a New Concept of Universal Host for Improved Efficiency and Lifetime in Red, Yellow, Green, and Blue Phosphorescent Organic Light-Emitting Diodes. *Advanced Science* **2018**, *5* (2), 1700608.
(67) Xu, T.; Zhou, J.-G.; Huang, C.-C.; Zhang, L.; Fung, M.-K.; Murtaza, I.; Meng, H.; Liao, L.-S. Highly Simplified Tandem Organic Light-Emitting Devices Incorporating a Green Phosphorescence Ultrathin Emitter within a Novel Interface Exciplex for High Efficiency. *ACS Appl. Mater. Interfaces* **2017**, *9* (12), 10955−10962.
(68) Shibata, M.; Sakai, Y.; Yokoyama, D. Advantages and disadvantages of vacuum-deposited and spin-coated amorphous organic semiconductor films for organic light-emitting diodes. *J. Mater. Chem. C* **2015**, *3* (42), 11178−11191.
(69) Gupta, A. K.; Cordes, D. B.; De, J.; Slawin, A. M. Z.; Warriner, S.; Samuel, I. D. W.; Zysman-Colman, E. Deep-red to NIR solution-processed OLEDs of donor-decorated quinoxaline-based TADF aggregates. *J. Mater. Chem. C* **2025**, *13* (12), 6123−6135.
(70) Wang, H.; Zhao, B.; Qu, C.; Duan, C.; Li, Z.; Ma, P.; Chang, P.; Han, C.; Xu, H. 2,3-Dicyanopyrazino phenanthroline enhanced charge transfer for efficient near-infrared thermally activated delayed fluorescent diodes. *Chem. Eng. J.* **2022**, *436*, 135080.

https://doi.org/10.1021/acsaom.5c00340
ACS Appl. Opt. Mater. 2025, 3, 2583−2594